Irradiance-based calibration and validation of MODIS visible and near-infrared channels

GONG Hui[1,2], **TIAN Guoliang**[1], **YU Tao**[1], **ZHANG Yuxiang**[3], **GU Xingfa**[1], **GAO Hailiang**[1]

1. *State Key Laboratory of Remote Sensing Science*, *Jointly Sponsored by the Institute of Remote Sensing Applications of Chinese Academy of Sciences and Beijing Normal University*, *Beijing* 100101, *China*;
2. *School of Civil Engineering*, *Beijing Jiaotong University*, *Beijing* 100044, *China*;
3. *National Satellite Meteorological Center*, *China Meteorological Administration*, *Beijing* 100081, *China*

Abstract: Radiometric calibration is the key of improving quality and quantitative applications of the remote sense data. A irradiance-based radiometric calibration campaign was performed by National Spaceborne Demonstration at the Erenhot test site on June 1, 2007, in which Terra MODIS was the object. It showed that the irradiance-based calibration results were in good agreement with both the MODIS on-board calibration and reflectance-based calibration results with the variations less than 3.3% at the site. It was concluded that the irradiance-based calibration method was performed correctly, while the differences among the coefficients showed that the measurement of the ratio of diffuse-to-global ratio has crucial impact on results of irradiance-based calibration. The results from different aerosol modes confirmed that the irradiance-based radiometric calibration can reduce the error caused by the assumption of the aerosol mode.

Key words: radiometric calibration, calibration coefficient, irradiance-based method, MODIS

CLC number: TP701/P407 **Document code:** A

Citation format: Gong H, Tian G L, Yu T, Zhang Y X, Gu X F and Gao H L. 2010. Irradiance-based calibration and validation of MODIS visible and near-infrared channels. *Journal of Remote Sensing*. **14**(2): 207—218

1 INTRODUCTION

Since the 1990s, with the deep development of satellite technique and the need of remote sensing monitoring of global resource, environment change and disasters, great importance was gradually attached to quantitative research of remote sensing data (Qiu, 2001). The fundamental prerequisite and the key link for quantification of remote sensing lie to absolute radiometric calibration, that is to say, digital counts recorded by a sensor should be transferred into radiance value (Tian, 1999). The accuracy of radiometric calibration directly affects quality of quantitative remote sensing products. Radiometric calibration methods in the world include prelaunch calibration, onboard calibration and vicarious calibration (Dinguirard & Slater, 1999). For the sensor without onboard calibrator, vicarious calibration is an effective method not only for improving quality of remote sensing data but also for realizing quantification of remote sensing. Even with onboard calibrator, it cannot completely detect calibration shifts caused by possible sensor changes (Li, 2006), Vicarious calibration should still be required to ascertain response change of sensors in order to ensure reliability and accuracy of quantitative application of remote sensing. Slater *et al*. (1987) proposed vicarious calibration methods which have been proved to be highly accurate and effective (Gu, 2000). These methods include reflectance-based calibration method, radiance-based calibration method and irradiance-based calibration method (Biggar, 1990). Reflectance-based method depends on ground-based measurements including surface reflectance measurement, atmospheric extinction measurement and radiosonding observation at the sensor overpass. These measurement data are inputted to a radiative transfer model to obtain the entrance pupil radiance of the sensor (Slater *et al*., 1987). Due to its relatively easy operation and the high accuracy of 3.6% in the visible and infrared bands (Thome, 1999a), the method is put into use extensively. However its numerous assumptions about refractive index and particle size distribution of aerosols in the atmosphere bring great systematic error. Radiance-based method was based on a calibrated radiometer flown in an aircraft at high altitude to measure the radiance of the ground target. Then the radiance is corrected for the residual atmospheric effect to give the entrance pupil radiance (Slater *et al*., 1987). It is the most accurate one of the three methods due to the high precision capability of 2.5% (Thome, 1999a). Yet it fails to be applied widely

Received: 2008-09-24; **Accepted**: 2009-02-10

Foundation: National High Technology Research and Development Program (863 program) of China (No. 2006AA12Z113)

First author biography: GONG Hui (1971—), female, doctoral student. She got master degree in Changchun University of Science and Technology in 1999. Her research interest is radiometric calibration and quantitative remote sensing. Currently, 5 representative papers haven been published. E-mail: gonghuiyue@sohu.com

© 1994-2012 China Academic Journal Electronic Publishing House. All rights reserved. http://www.cnki.net

owing to its great cost as well as many requirements and limitations during the measurement. Irradiance-based method improves the reflectance-based method. In addition to the requirement of all ground measurements of the reflectance-based method, it adds measurements of the downwelling diffuse-to-global ratios to determine the scattering characteristic of aerosol from which the error caused by these assumptions is reduced (Biggar, 1990) and calibration accuracy is improved to 2.9% (Thome, 1999a). The method was used to calibrate some sensors including SPOT HRV, Landsat-5 TM, MODIS, CBERS-1 CCD and FY-1C satellite sensor (Thome, 1999a; Thome *et al*., 1997b; Biggar *et al*., 1991; Zhang *et al*., 2002; Hu *et al*., 2003), but it is not used extensively at present.

The work planed to discuss the irradiance-based method. Since there was perfect onboard calibrators on MODIS and the its calibration accuracy could reach ±2% (Xiong & Barnes, 2006), onboard calibration result could be used to verify the accuracy of the irradiance-based method. Thus, visible and infrared bands of Terra MODIS were chosen as an object in the campaign and irradiance-based calibration was performed at the Erenhot test site in June 2007.

2 METHOD AND EXPERIMENT

2.1 Reflectance-based calibration method

The entrance pupil radiance $L_\lambda(\theta_s,\theta_v,\varphi_s,\varphi_v)$ of wavelength λ could be expressed as the apparent reflectance $\rho_\lambda^*(\theta_s, \theta_v, \varphi_s, \varphi_v)$ by (Biggar, 1990)：

$$\rho_\lambda^*(\theta_s,\theta_v,\varphi_s,\varphi_v)=\pi L_\lambda(\theta_s,\theta_v,\varphi_s,\varphi_v)d^2/E_{0\lambda}\mu_s \tag{1}$$

where $E_{0\lambda}$ was the extra-atmospheric solar spectral irradiance at the mean distance of the earth and sun, θ_s, θ_v, φ_s, φ_v was respectively the solar and view zenith and azimuth angles, d was the earth-sun factor and μ_s was the cosine of the sun zenith angle.

For a uniform lambertian ground of surface reflectance ρ, the apparent reflectance $\rho^*(\theta_s, \theta_v, \varphi_s, \varphi_v)$ was given by the equation (Biggar, 1990):

$$\rho^*(\theta_s,\theta_v,\varphi_s,\varphi_v)=\rho_A(\theta_s,\theta_v,\varphi_s,\varphi_v)+\frac{(\tau(\mu_s)\cdot\rho\cdot\tau(\mu_v))}{(1-\rho s)} \tag{2}$$

where $\rho_A(\theta_s, \theta_v, \varphi_s, \varphi_v)$ was the upward scattering reflectance of the atmosphere, s was the spherical albedo of the atmosphere and τ was respectively the global atmospheric transmittance. $\tau(\mu_s)$ could be defined as (Biggar, 1990)

$$\tau(\mu_s)=e^{-\delta/\mu_s}+\frac{\int_0^{2\pi}\int_0^1 L^0(\mu_v,\mu_s,\varphi,\varphi_s)\mu d\mu d\varphi}{\mu_s E_s}=e^{-\delta/\mu_s}+\frac{E_d{}^0}{\mu_s E_s} \tag{3}$$

where L^0 and E^0 were respectively the downward radiance and irradiance caused by the scattering process at the ground level where the ground reflectance was zero and δ was total atmospheric optical depth. Fig. 1 was the irradiance composition at ground level.

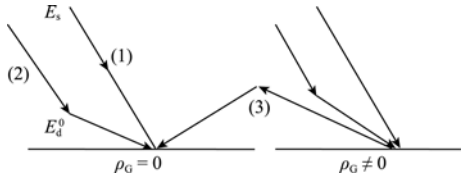

(1) Direct irradiance at ground level= $\mu_s E_s e^{-\delta/\mu_s}$; (2) Intrinsic atmospheric irradiance=$E^0{}_d$; (3) Coupled ground-atmosphere irradiance= $\mu_s E_s \frac{\tau(\mu_s)}{1-\rho s}$

Fig. 1 Irradiance decomposition

The diffuse-to-global ratio at θ_s could be written as (Biggar, 1990):

$$\alpha_s=\frac{E_d(\mu_s)}{E_G(\mu_s)}=\frac{E_d(\mu_s)}{\mu_s E_s e^{-\delta/\mu_s}+E_d(\mu_s)} \tag{4}$$

where $E_G(\mu_s)$ was the global irradiance, $E_d(\mu_s)$ was respectively the diffuse irradiance which included the intrinsic diffuse irradiance $E^0{}_d(\mu_s)$ and also the coupling term between atmosphere and ground for both the direct team and the diffuse component. $E_d(\mu_s)$ could be shown to be (Biggar, 1990):

$$E_d(\mu_s)=\frac{1}{1-\rho s}[E^0{}_d(\mu_s)+\mu_s E_s e^{-\delta/\mu_s}\rho s] \tag{5}$$

Inserting Eq. (4)and (5) into Eq. (3), $\tau(\mu_s)$ could be rewritten as (Biggar, 1990):

$$\tau(\mu_s)=\frac{(1-\rho s)e^{-\delta/\mu_s}}{1-\alpha_s} \tag{6}$$

According to the reciprocity theorem, $\tau(\mu_v)$ could be correspondingly expressed as (Biggar, 1990):

$$\tau(\mu_v)=\frac{(1-\rho s)e^{-\delta/\mu_v}}{1-\alpha_v} \tag{7}$$

where α_v was the diffuse-to-global ratio at θ_v. Eq. (2) could then be written as (Biggar, 1990):

$$\rho^*(\theta_s,\theta_v,\varphi_s,\varphi_v)=\rho_A(\theta_s,\theta_v,\varphi_s,\varphi_v)+\frac{e^{-\delta/\mu_s}}{1-\alpha_s}\rho(1-\rho s)\frac{e^{-\delta/\mu_v}}{1-\alpha_v} \tag{8}$$

2.2 Experiment

2.2.1 *The test site*

The Erenhot test site, which is fairly wide and flat, is located at southeast of Erenhot city (Fig. 2). The ground surface is covered by coarse sand whose compositions are mainly light-colored minerals. It has low vegetation coverage with short sedges and camel thorns. The surface is highly bright and homogeneous.

2.2.2 *Surface spectra measurements*

Surface spectra measurements were performed at the site at the time of Terra MODIS overpass on June 1, 2007. The Analytical Spectral Devices (ASD) Spectrometer was used to obtain the surface spectra. The spectrometer combines three spectrometers to cover the entire solar reflected wavelength range

© 1994-2012 China Academic Journal Electronic Publishing House. All rights reserved. http://www.cnki.net

Fig. 2 The test site

from 350nm to 2500nm with approximately 3 nm (VNIR) and 10 nm (SWIR) spectral resolution (David, 2002).

An area of about 2km×2km at the site was chosen for real-time measurement. Thanks to its uniformity and limit of measurement time, the area was broken into 42 sub-areas that were 6 lines ×7 samples and 42 samples were collected. The measurement sequence of spectra for every sample were two readings for panel, ten for surface and then two new readings for panel again. In order to reduce the influence of solar irradiance change to the field measurement as much as possible, measurement for every sample was finished during 1min. At the same time, a global positioning system (GPS) receiver was used to precisely identify the ASD locations at each sample point. It took 2h to collect spectra data for the whole site. About 554 spectra data were collected for the whole site.

2.2.3 *Atmospheric characteristic measurements*

During the day of the field measurement, atmospheric measurements were made to obtain atmospheric total optical depth, aerosol optical depth, content of ozone and total column water vapor. An automatic sun tracking photometer, CE318, was arranged to automatically receive spectral solar direct irradiance data from seven in the morning to nineteen in the evening at the location 2 km away from the test site. Atmospheric aerosol optical depth was then derived from the measurement data. The instrument has eight bands (Yuan *et al.*, 2006). Three radiosonding observations were performed at the whole day and total column water vapor was then obtained with sounding view outline. The content of ozone came from NASA TOMS data (Richard, 2008).

2.2.4 *Diffuse-to-global ratio measurements*

The diffuse-to-global ratio measurement was required in the irradiance-based method. In addition to a reference panel, A portable HandHeld spectroradiometer whose wavelength range was from 325nm to 1075nm (David, 2002) was used to obtain the diffuse-to-global ratio. Owing to the limitation of spectrometer's spectral range, only first four bands of MODIS could be calibrated. For the reference panel being nearly lambertian, the irradiance $E(\mu_s)$ was proportional to the panel radiance $L(\mu_s)$ measured at nadir (Biggar, 1990). The diffuse-to-global ratio could be got by the following

$$\frac{E_d(\mu_s)}{E_G(\mu_s)} = \frac{L_d(\mu_s)}{L_G(\mu_s)} \tag{9}$$

The diffuse-to-global ratio measurement was made every 10min and continued from 7:30 a.m. to 19:00 p.m. Before and after 30min of the MODIS overpass, the measurement was changed to be made every 5min. For every measurement, total radiance L_{G1} just above a reference panel was first measured with the spectroradiometer. The spectroradiometer should be placed at the distance above the reference panel where it could be insured that the panel was full of its field of view and there was no shade of the spectroradiometer on the panel. Secondly, a block panel was moved into position to just shadow the reference panel in order to remove direct solar beam to get diffuse radiance L_d. Then the block panel was moved aside and a new total radiance reading L_{G2} was taken. So diffuse-to-global ratio at the measurement could be obtained by dividing L_d with average value of L_{G1} and L_{G2}.

3 DATA PROCCESSING AND RESULT ANALYSIS

3.1 Surface spectral qdata processing and analysis

For each 42 samples, ten surface measurement data and four panel data were respectively averaged to get average surface and panel measurement values at the location of the sample. BRF of the panel were interpolated according to measurement times to compute its spectral reflectance at the surface measurement time. Then absolute spectral reflectance of the sample could be given by Eq. (10).

$$\rho(\lambda) = \frac{v_T(\lambda)}{v_s(\lambda)}\rho_S(\lambda) \tag{10}$$

where $\rho_s(\lambda)$ was spectral reflectance of the panel, $v_s(\lambda)$ and $v_T(\lambda)$ were respectively raw digital counts of panel and target on the same view condition.

A representative spectral reflectance for the site at the time of MODIS overpass on June 1, 2007 was obtained after averaging all spectral reflectance of 42 ground samples, which was shown in Fig. 3. It was obviously seen that spectral reflectance for MODIS visible and infrared bands was from 0.1 to 0.4 and it increased stably and slowly with wavelength. Average relative error 3.1% of spectral reflectance was in the range from 350nm to 1100nm. The fact noted that surface reflectance of the site existed little dispersion and fairly homogenous. By comparison between average surface reflectance for 42 samples

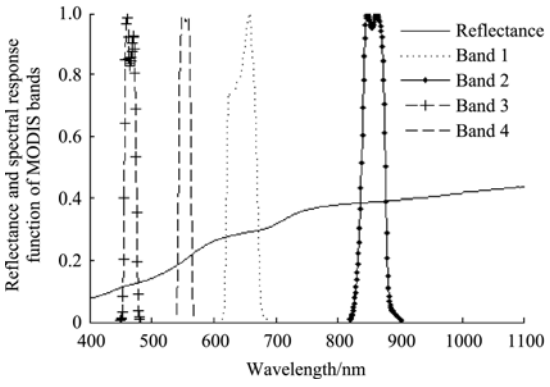

Fig. 3 Surface reflectance results of the test site and spectral response function of MODIS

© 1994-2012 China Academic Journal Electronic Publishing House. All rights reserved. http://www.cnki.net

derived from the whole measurement time and reflectance obtained just at the MODIS overpass time, their relative error was only 0.3%. It was indicated that average surface reflectance derived from the whole measurement time could be representative of surface reflectance of the site. The average spectral reflectance was then changed into the equivalent spectral reflectance corresponding to MODIS band by using the spectrum matching between surface spectra data and MODIS band. The error of equivalent spectral reflectance was 0.004—0.02 and its average accuracy was 3.3%.

3.2 CE318 data processing and result analysis

According to spectral solar direct irradiance and diffuse irradiance received with CE318, total and atmospheric aerosol optical depth corresponding to CE318 channel was determined using a Langley method. Its error was about 0.5%. Fig. 4(a) showed Lanley-plot result of CE318's data. It was noted that Lanley plot kept obviously linear and aerosol content existed little change from 7:30 to 19:00 which indicated that atmosphere was very stable. Fig. 4(b) showed Ångström turbidity coefficient, β, and wavelength exponent, α. It could be noted from Fig. 4(b) that aerosol composition was mainly large particles the concentration of aerosol was very low. It indicated that the atmosphere was clean and sunny during the day and aerosol had little influence on atmospheric radiative transfer. A series of total optical depth extracted during the period of a.m. were interpolated to obtain the total optical depth at the MODIS overpass according to its overpass time. The value then was integrated with spectral response function of MODIS to achieve equivalent total optical depth of MODIS band.

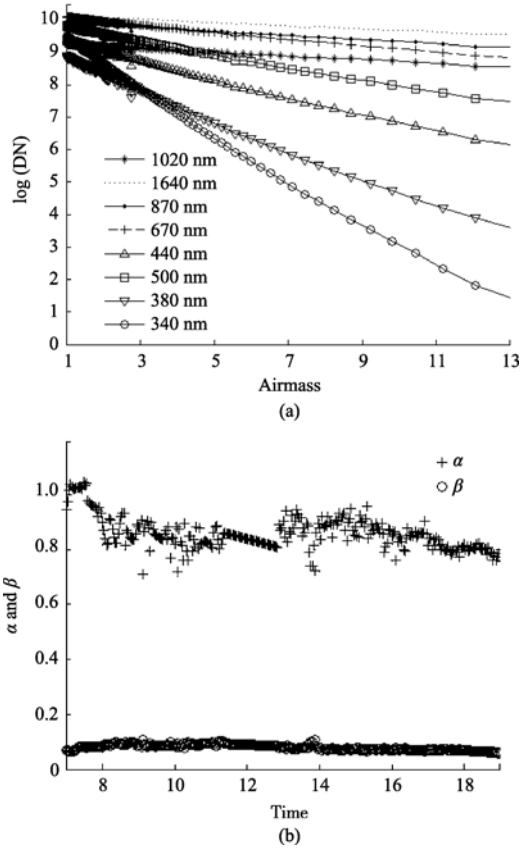

Fig. 4 Optical properties of atmospheric aerosol on June 1, 2007
(a) Lanley-plot result of CE318's data; (b) Angstrom parameters

3.3 Diffuse-to-global ratio computation and analysis

Main parameters for irradiance-based method were diffuse-to-global ratio θ_s and θ_v. For the case of satellite observation when diffuse-to-global ratio measurement was not made at exactly the MODIS overpass, we could interpolate a value for α_s at θ_s. When the sensor view angle was so small that it wasn't in the range of solar zenith angles, we should extrapolate a series of measurements to the required angle θ_v (Biggar, 1990).

$$\log\left(\frac{E_D}{E_G}\right) = \log(1-\alpha) = \log(1-\rho s) - (1-b)\delta / \mu_S \qquad (11)$$

where $1/\mu_s$, the inverse of the cosine of the sun zenith angle, was airmass which was usually expressed as m. The preceding equation then could be simplified as linear formula $y=y_0+cm$, where slope, c, was $-(1-b)\delta$; intercept, y_0, was log $(1-\rho s)$. Atmospheric stability should be decided at first. A log plot of the data (log $(1-\alpha)$ versus m) was shown in Fig. 5. It showed that value of log $(1-\alpha)$ increased as airmass decreased, in other words, diffuse-to-global ratio decreased as airmass decreased. It indicated the fact that atmosphere was stable which agreed with the CE318 result. Thus α_s and α_v could be calculated by using the fitted slope value.

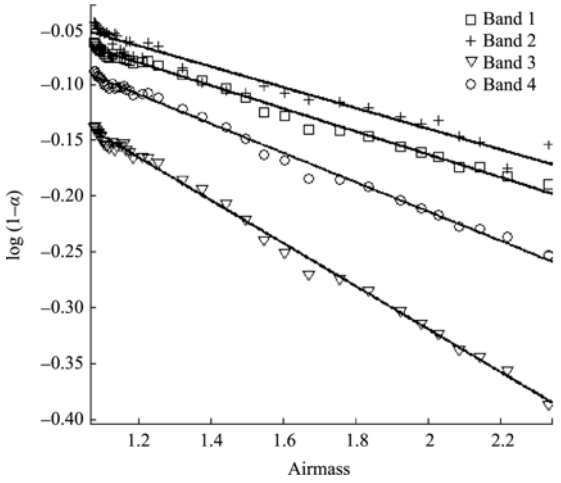

Fig. 5 The log plot of the data (log $(1-\alpha)$ versus m) on June1, 2007

3.4 Calibration coefficients calculation and analysis

Since the parameters were obtained which included equivalent spectral reflectance, aerosol optical depth, total column water vapor, content of ozone and geometric condition, they could be input to a radiative transfer model, 6S, to calculate values for the upward scattering reflectance (ρ_A) and the spherical albedo (S) of the atmosphere. Then the parameters required in Eq. (8) were substituted into the equation to

© 1994-2012 China Academic Journal Electronic Publishing House. All rights reserved. http://www.cnki.net

estimate apparent reflectance of MODIS band. On the other hand, the area in the MODIS image corresponding to the measurement site was then precisely selected according to GPS data and the average digital count was extracted by averaging the output for MODIS imagery pixels. Since offset of MODIS visible and infrared band was 0, calibration coefficient could be got by the relation between average digital count and apparent reflectance corresponding to the same MODIS band and the same area as the following.

$$\rho_i = C_i \times \mathrm{DC}_i \tag{12}$$

Where ρ_i was apparent reflectance corresponding to MODIS band i, DC_i was average digital count of MODIS band i and C_i was calibration coefficient for MODIS band i.

The result of irradiance-based method could be verified with onboard calibration regarded as a standard value and it was compared with the reflectance-based result. Table 1 showed calibration coefficients of MODIS obtained by irradiance-based method, reflectance-based method and onboard method.

Table 1 Comparison of results among the irradiance-based, the reflectance-based and on-board calibrations for Terra-MODIS on June 1, 2007

	Band 1	Band 2	Band 3	Band 4
ρ_{TOA} from irradiance-based method	0.249	0.344	0.150	0.185
ρ_{TOA} from reflectance-based method	0.253	0.351	0.154	0.189
ρ_{TOA} from onboard method	0.250	0.355	0.152	0.189
C_{i} from irradiance-based method /$\times 10^{-5}$	5.25	3.17	3.78	3.4
C_{i} from reflectance-based method / $\times 10^{-5}$	5.33	3.24	3.87	3.46
C_{i} from onboard method / $\times 10^{-5}$	5.27	3.27	3.82	3.47
Error between irradiance-based method and onboard method (%)	−0.392	−3.244	−0.872	−2.080
Error between reflectance-based method and onboard method (%)	0.999	−1.009	1.304	−0.247

It was noted from Table 1 that TOA reflectance calculated from irradiance-based method was in quite good agreement with onboard calibration and reflectance-based results and the error between irradiance-based method and onboard method was less than 3.3%, which proved the accuracy of the irradiance-based method. The apparent reflectance from irradiance-based method was the lowest of three methods and the error between irradiance-based method and reflectance-based method of band 2 and band 4 were larger than that of band 1 and band 3. It is because that operation error of diffuse irradiance measurement coming from block panel in the course of diffuse-to-global measurements made the measured diffuse irradiance turns small. In other words, it made diffuse-to-global ratio turned small. As a result, the apparent reflectance turned small. While diffuse-to global values of band 2 and band 4 were relatively smaller than other two bands, which contributed to larger errors of the two bands. All the above confirmed that diffuse-to-global measurements were critical to the accuracy of the irradiance-based the method. It was advised that using more accurate instrument to measure diffuse-to-global ratio could improve the accuracy of the method.

In order to study a difference in the effect of assumption of aerosol model on both the irradiance-based method and the reflectance-based method, several models were selected to estimate the apparent reflectance based on the measurement data at the Erenhot test site on June 1. They involved desertic model, continental model and urban model. The result was shown in Fig. 6. Table 2 showed relevant calibration coefficients. It could be seen from Fig. 6 and Table 2 that results respectively achieved from irradiance-based method and the reflectance-based method underwent dissimilar effects under three different models. For all three models, apparent reflectances varied slightly since their difference was only 0.25% and relative errors were from 0.39% to 3.78%. As assumption of aerosol model only affected ρ_{A} and S while values of the two parameters were quietly small, using the value of diffuse-to-global ratio in place of assumption of aerosol model made the effect of assumption of aerosol model on the result of the irradiance-based method drop to the low level. However the results obtained by reflectance-based method changed violently owing to the influence of diverse aerosol models. The difference between apparent reflectances reached 1.7% and relative error drifted from 0.47% to 8.96%. Apparent reflectance derived from urban model lied the lowest because of its strong absorption. It is distinctly proved that the irradiance-based method could reduce the error come from hypothesis of aerosol model.

Table 2 showed calibration coefficients derived from different aerosol model. It could be seen that calibration coefficients respectively achieved from irradiance-based method and the reflectance-based method underwent dissimilar effects under desertic model, continental model and urban model. For all three models, calibration coefficient obtained by irradiance-based method varied slightly from 0.39% to 3.78%, while

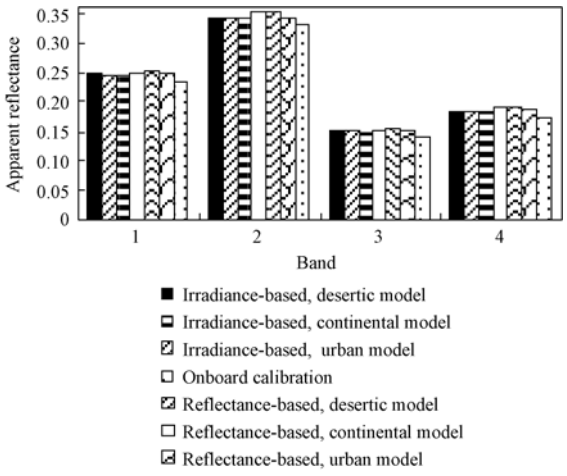

Fig. 6 Comparison of TOA reflectances between the irradiance-based and the reflectance-based from three aerosol modes

© 1994-2012 China Academic Journal Electronic Publishing House. All rights reserved. http://www.cnki.net

Table 2 Comparison of calibration coefficients between the irradiance-based and the reflectance-based from three aerosol modes

Calibration coefficients	Irradiance-based, desertic model /$\times10^{-5}$	5.25	3.17	3.78	3.40
	Irradiance-based, continental model / $\times10^{-5}$	5.22	3.15	3.78	3.38
	Irradiance-based, urban model / $\times10^{-5}$	5.19	3.15	3.71	3.35
	Onboard calibration / $\times10^{-5}$	5.27	3.27	3.82	3.47
	Reflectance-based, desertic model / $\times10^{-5}$	5.33	3.24	3.87	3.46
	Reflectance-based, continental model / $\times10^{-5}$	5.24	3.18	3.83	3.40
	Reflectance-based, urban model / $\times10^{-5}$	4.92	3.04	3.54	3.16
Error between irradiance-based calibration and onboard calibration (%)		0.39—1.51	3.19—3.78	0.87—2.69	2.05—3.35
Error between reflectance-based calibration and onboard calibration (%)		0.6—6.71	2.88—6.98	0.47—7.34	1.93—8.96

calibration coefficient obtained by reflectance-based method changed violently from 0.47% to 8.96%. It is further proved that the irradiance-based method could reduce the error come from hypothesis of aerosol model.

4 CONCLUSION

According to the irradiance-based radiometric calibration of Terra MODIS visible and infrared bands performed at the Erenhot test site on June 1, 2007, some conclusions could be obtained as following.

(1) Calibration coefficients for MODIS bands on June 1, 2007 were successfully achieved by using irradiance-based calibration method. It was shown by comparison of three calibration methods: onboard calibration, reflectance-based and irradiance-based methods, that the result from irradiance-based method was quietly consistent with the two other methods with the relative error of 3.3%. The conclusion affirmed that the irradiance-based was accurate.

(2) As for the irradiance-based method, the diffuse-to-global ratio measurement was a key factor to the accuracy of the method.

(3) In the irradiance-based method, the assumption of aerosol model was replaced by diffuse-to-global ratio measurement value. Since the assumption of aerosol model only had effect on the determination of ρ_A and s, the replacement could reduce the error caused by the assumption of aerosol model.

(4) The paper provided a systemic experiment procedure for radiometric calibration of optical remote sensing using irradiance-based method.

Acknowledgements: The authors are grateful to Wei Feiming, Fu he, Zhu Li, Hu Mei, guo ding and Xiao Dantao of Institute of remote sensing Applications for their great help in the field campaign and hu Xiuqing of National Satellite Meteorological Center for his kindly help in data processing.

REFERENCES

Biggar S F. 1990. Cross Methods for Satellite Sensor Absolute Radiometric Calibration. America: the University of Arizona

Biggar S F, Dinguirard M C, Gellman D I, Henry P, Jackson R D, Moran M S and Slater P N. 1991. Radiometric calibration of SPOT 2 HRV: a comparison of three methods. Proc.SPIE, **1493**: 155—162

David C H. Analytical spectral devices.2002. Inc. HandHeld Spectroradiometer User's Guide

Dinguirard M and Slater P N. 1999. Calibration of space-multispectral imaging sensors: a review. *Remote Sensing of Environment*, **68**: 194—205

Gu M L. 2000. In-flight absolute radiometric calibration of satellite remote sensor. Spacecraft Recovery & Remote Sensing, **21**(1): 16—21

Hu X Q, Zhang Y X and Qiu K M. 2003. In-flight radiometric calibration for VIR channels of FY-1C satellite sensor by using irradiance-based method. *Journal of Remote Sensing*, **7**(6): 458—464

Li X Y. 2006. In Flight Radiometric Calibration and Pixel Based Calibration for CCD Camera and WFI Imager on CBERS-02. Beijing: Chinese Academy of Sciences

Qiu K M. 2001. Constructions, Scientific fruits and applied foreground of Chinese satellite radiometric calibration sites. Corpus Chinese Remote Sensing Satellites Radiometric Calibration Sites Contribution. Beijing: Ocean Press

Richard D M. What is the total column ozone amount over your house?http://toms.gsfc.nasa.gov/teacher/ozone_overhead_v8.html. (2008-09-09)

Slater P N, Biggar S F, Holm R G, Jackson R D, Mao Y, Moran M S, Palmer J M and Yuan B. 1987. Reflectance- and radiance-based methods for the cross absolute calibration of multispectral sensors. *Remote Sensing of Environment*, **22**(1): 11—37

Thome K J. 1999a. Validation plan for MODIS level 1 at-sensor radiance. (http://modis.gsfc.nasa.gov/data/atbd/val_atbd.php) (2008-09-09)

Thome K J, Crowther B G and Biggar S F. 1997b. Reflectance- and irradiance-based calibration of Landsat-5 Thematic Mapper. *Canadian Journal of Remote Sensing*, **23**: 309—317

Tian Q J. 1999. Quantitative theory, Method and application of remote sensing information. China Science & Technology Publishing House

Xiong X and Barnes W. 2006. An overview of MODIS radiometric calibration and characterization. *Advances in Atmospheric Sciences*, **23**(1): 69—79

Yuan H J, Gu X F, Chen L F Yu T, Liu Q and Li X W. 2006. Retrieval and analysis of aerosol optical thickness over Qianyanzhou Region. *Journal of Remote Sensing*, **10**(5): 762—769

Zhang D Y, Qiao Y L, Yi W N. Yang S Zh, Meng F G, Wu H Y and Zhang J P. 2002. The irradiance-based method research of experimentation on radiometric calibration site-the comparison of synchronous observing instruments. *Optoelectronic Technology & Information*, **15**(3): 9—13

© 1994-2012 China Academic Journal Electronic Publishing House. All rights reserved. http://www.cnki.net

MODIS 辐照度法定标试验研究

巩　慧[1,2], 田国良[1], 余　涛[1], 张玉香[3], 顾行发[1], 高海亮[1]

1. 遥感科学国家重点实验室, 中国科学院　遥感应用研究所, 北京　100101;
2. 北京交通大学 土建学院, 北京　100044;
3. 中国气象局 国家卫星气象中心, 北京　100081

摘　要: 利用内蒙古二连浩特实验场对 Terra 卫星 MODIS 传感器开展辐照度基定标方法研究。定标结果表明,辐照度法定标系数和 MODIS 的星上定标、反射率基法定标系数非常接近, 相对差异<3.3%, 证明辐照度基定标方法正确。定标系数之间的差异说明, 漫射辐射与总辐射辐照度比测量的精度对辐照度法结果影响很关键。不同气溶胶模式下得到的结果说明辐照度法可以减小因气溶胶模式的假设产生的误差。

关键词: 辐射定标, 定标系数, 辐照度基法, MODIS

中图分类号: TP701/P407　　文献标识码: A

引用格式: 巩　慧, 田国良, 余　涛, 张玉香, 顾行发, 高海亮. 2010. MODIS 辐照度法定标试验研究. 遥感学报, **14**(2): 207—218
Gong H, Tian G L, Yu T, Zhang Y X, Gu X F and Gao H L. 2010. Irradiance-based calibration and validation of MODIS visible and near-infrared channels. *Journal of Remote Sensing*. **14**(2): 207—218

1　引　言

20世纪90年代以来, 随着卫星技术和遥感应用技术定量化的深入和发展以及全球资源、环境变化和灾害遥感监测的需求, 卫星遥感数据的定量化研究日益受到重视(邱康睦, 2001)。遥感定量化的基本前提和关键在于传感器的绝对辐射定标, 即将传感器记录的数字值转换成对应像元地物的实际辐射亮度值(田庆久, 1999), 辐射定标精度直接影响各种定量遥感产品的质量。国际上采用的辐射定标方法包括发射前的实验室定标、星上定标以及发射后利用地面目标进行的在轨定标方法等(Dinguirard & Slater, 1999)。对于没有星上定标系统的传感器, 在轨定标是提高卫星遥感数据的质量和实现卫星遥感定量化的有效手段; 即使卫星上有内定标系统, 也不能完全确定传感器的衰减变化导致的定标结果的改变(李小英, 2006), 依然需要通过在轨定标订正传感器特性的变化, 确保遥感数据定量应用的可靠性和准确度。以美国亚利桑那大学光学科学中心 Slater 教授为代表的科学家于 20 世纪 70 年代提出的场地辐射定标法(Slater, 1987)是获取传感器入瞳处的辐亮度精度较高、行之有效的方法(顾名澧, 2000), 包括反射率法、辐照度法和辐亮度法等 3 种方法(Biggar, 1990)。反射率法是在卫星经过地表上空时, 准同步进行场地表面反射比测量、大气消光测量和探空观测, 将地表和大气参数输入辐射传输模型, 获得卫星传感器入瞳处的辐亮度(Slater 等, 1987)。反射率法操作相对简便, 在可见和近红外波段的校正精度可达 3.6%(Thome, 1999a), 应用最广。但由于反射率法对气溶胶模式(如气溶胶折射指数和粒子谱分布)的一些近似假设而带来较大的系统误差。辐亮度法是将一个标定好的辐射计携带到高空, 与需要标定的传感器几乎同时、相同观测条件下观测地表, 通过对辐射计和传感器高度间的大气影响进行订正, 获得卫星入瞳处的辐亮度(Slater 等, 1987)。辐亮度法是 3 种方法中最精确的方法, 其精度可达 2.5% (Thome, 1999a), 但由于耗费大及实施过程中的很多限制, 这种方法无法得到广泛应用。辐照度法改进了反射率法, 它除了需要进行反射率法所有的测量项目外, 还增加测量地面的漫射辐射与总辐照度比值描述大气胶的散射特性, 减小了反射率法中由于气溶胶模式假设带来的误差(Biggar, 1990), 可将

收稿日期: 2008-09-24; 修订日期: 2009-02-10

基金项目: 国家 863 无场地定标关键技术项目(编号: 2006AA12Z113)。

第一作者简介: 巩慧(1971—), 女, 博士研究生, 1999 年毕业于长春科技大学, 目前主要从事定量遥感方面的研究工作。E-mail: gonghuiyue@sohu.com。

© 1994-2012 China Academic Journal Electronic Publishing House. All rights reserved.　http://www.cnki.net

定标精度提高到 2.9% (Thome, 1999a)。这种方法曾用于 SPOT 的 HRV、Landsat-5 的 TM、MODIS、CBERS-1 卫星 CCD 相机以及 FY-1C 上传感器的定标(Thome 等, 1999a, 1997b; Biggar 等, 1991; 张冬英等, 2002; 胡秀清等, 2003), 但目前还没有得到广泛应用。

本次工作拟对辐照度法进行方法研究, 由于 MODIS 具有完善的星上定标系统, 星上定标系数的不确定性达±2%(Xiong & Barnes, 2006), 利用星上定标检验辐照度法的正确性, 以 Terra 卫星 MODIS 传感器的可见光-近红外波段为对象, 于 2007 年 6 月在二连浩特实验场地进行辐照度法定标研究。

2 方法和实验

2.1 辐照度基辐射定标方法

卫星传感器从空间测量波长 λ 处的辐亮度 $L_\lambda(\theta_s,\theta_v,\varphi_s,\varphi_v)$ 可以表示为表观反射率(Biggar, 1990):

$$\rho_\lambda^*(\theta_s,\theta_v,\varphi_s,\varphi_v)=\pi L_\lambda(\theta_s,\theta_v,\varphi_s,\varphi_v)d^2/E_{0\lambda}\mu_s \quad (1)$$

式中, $E_{0\lambda}$ 为大气层外的太阳谱辐照度, θ_s、θ_v、φ_s、φ_v 分别为太阳的和观测的天顶角和方位角, d 为平均与实际日—地距离之比, $\mu_s=\cos(\theta_s)$。

对于反射率为 ρ 均匀的朗伯地表面, 其表观反射率为(Biggar, 1990):

$$\rho^*(\theta_s,\theta_v,\varphi_s,\varphi_v)=\rho_A(\theta_s,\theta_v,\varphi_s,\varphi_v)+\frac{(\tau(\mu_s)\cdot\rho\cdot\tau(\mu_v))}{(1-\rho s)} \quad (2)$$

式中, $\rho_A(\theta_s,\theta_v,\varphi_s,\varphi_v)$ 为大气本身产生的向上的程辐射反射率; ρ 为地表反射率; s 为大气半球反照率; $\tau(\mu_s)$与 $\tau(\mu_v)$分别为太阳—目标与目标—传感器路径上的总透过率。$\tau(\mu_s)$可以表示为(Biggar, 1990):

$$\tau(\mu_s)=e^{-\delta/\mu_s}+\frac{\int_0^{2\pi}\int_0^1 L^0(\mu_v,\mu_s,\varphi,\varphi_s)\mu d\mu d\varphi}{\mu_s E_s}=e^{-\delta/\mu_s}+\frac{E_d^0}{\mu_s E_s} \quad (3)$$

式中, L^0 和 E_d^0 分别为仅由散射过程产生的到达地面的辐亮度和辐照度,对应于地面反射率为零的情况, δ 为总的大气光学厚度。图 1 为地面接收的辐照度图。

太阳方向漫射辐射与总辐射之比可定义为(Biggar, 1990):

$$\alpha_s=\frac{E_d(\mu_s)}{E_G(\mu_s)}=\frac{E_d(\mu_s)}{\mu_s E_s e^{-\delta/\mu_s}+E_d(\mu_s)} \quad (4)$$

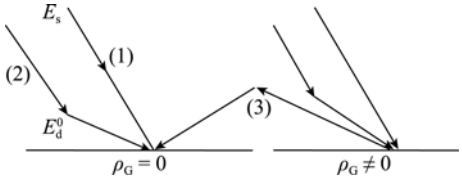

(1) 到达地面的太阳直接辐照度= $\mu_s E_s e^{-\delta/\mu_s}$; (2) 大气程辐射辐照度= E_d^0; (3) 大气—地面间耦合的辐照度= $\mu_s E_s \frac{\tau(\mu_s)}{1-\rho s}$

图 1 地面接收辐照度的各组成部分

式中, $E_d(\mu_s)$和 $E_G(\mu_s)$分别为漫射辐照度和总辐照度, $E_d(\mu_s)$包括大气的程辐射辐照度 $E_d^0(\mu_s)$以及大气和地面间对太阳直射光和漫射分量的耦合顶。漫射辐照度可表示为(Biggar, 1990):

$$E_d(\mu_s)=\frac{1}{1-\rho s}[E_d^0(\mu_s)+\mu_s E_s e^{-\delta/\mu_s}\rho s] \quad (5)$$

将式(4)、式(5)代入式(3), $\tau(\mu_s)$又可写为(Biggar, 1990):

$$\tau(\mu_s)=\frac{(1-\rho s)e^{-\delta/\mu_s}}{1-\alpha_s} \quad (6)$$

Biggar 根据互易定理, 将 $\tau(\mu_v)$可以相应地表示为(Biggar, 1990):

$$\tau(\mu_v)=\frac{(1-\rho s)e^{-\delta/\mu_v}}{1-\alpha_v} \quad (7)$$

式中, α_v 为观测方向漫射辐射与总辐射的辐照度之比。由此式(2)又可表示为(Biggar, 1990):

$$\rho^*(\theta_s,\theta_v,\varphi_s,\varphi_v)=\rho_A(\theta_s,\theta_v,\varphi_s,\varphi_v)+\frac{e^{-\delta/\mu_s}}{1-\alpha_s}\rho(1-\rho s)\frac{e^{-\delta/\mu_v}}{1-\alpha_v} \quad (8)$$

2.2 实验

2.2.1 场区介绍

二连浩特实验场位于内蒙古二连浩特市东南侧(图2), 面积广阔, 地势平坦, 地表层主要成分为以浅色矿物为主、含细砾的中粗砂, 亮度高, 表面均一, 有稀少低矮的茅草和骆驼刺, 覆盖度很低。

图 2 实验场地

© 1994-2012 China Academic Journal Electronic Publishing House. All rights reserved. http://www.cnki.net

2.2.2　地面光谱测量

根据 Terra 卫星过二连浩特实验场的轨道及过境时间，于 2007-06-01 在二连浩特实验场，利用 FR ASD 野外光谱仪进行准同步地面观测获取地表光谱数据。FR ASD 野外光谱仪光谱范围为 350—2500nm，光谱分辨率 VNIR 为 3nm; SWIR 为 10nm(David, 2002)。

在场区选择面积约为 2km×2km 的子区进行同步观测，根据场区均匀的特点以及时间的限制，将子区划分为 6×7 阵列，共选取 42 个采样点，对每个采样点进行 2 次参考板—10 次目标—2 次参考板的测量顺序测量地表光谱数据。为减少太阳辐照度变化对测值的影响，每个采样点在 1min 内完成测量。同时利用 GPS 对各同步采样点进行精确定位。同步观测时间为卫星过顶前后 1h，整个同步测区共获取 554 组有效光谱数据。

2.2.3　大气光学特性测量

地表光谱同步观测当天，在实验场区附近进行大气消光和气象探空观测，以获取实验场区上空气溶胶消光光学厚度、臭氧、水汽含量等大气光学特性参数。气溶胶光学厚度测量使用法国 CIMEL 公司的 CE318 自动跟踪太阳光度计，在距离场地 12km 处，自 7:30—19:00 采用等间隔时间自动测量太阳直射辐射强度。CE318 光度计有 8 个光谱波段(Yuan 等, 2006)。气象探空观测除常规 2 次探空观测外，在卫星过境时刻增加一次无线电探空观测。利用探空观测廓线，计算获得大气柱水汽含量(g/cm^2)。臭氧含量来自 NASA TOMS 数据(Richard, 2008)。

2.2.4　漫射辐射与总辐射比测量

辐照度法较反射率基法而言，还需要测量漫射辐射与总辐射比。测量仪器和参照物为手持式野外光谱仪(光谱范围 325—1075nm) (David, 2002)和漫反射标准板。由于光谱仪光谱范围的限制，只能对 MODIS 的 1—4 波段定标。对于近乎朗伯面的标准板，其表面的辐照度 $E(\mu_s)$正比于天底方向测量的标准板的辐射量 $L(\mu_s)$(Biggar, 1990)，因此漫射辐射与总辐射比可由下式得到:

$$\frac{E_d(\mu_s)}{E_G(\mu_s)}=\frac{L_d(\mu_s)}{L_G(\mu_s)} \tag{9}$$

测量时间从 7:30—19: 00，每间隔 10min 测量一次，卫星过境前后 30min 加密测量为 5min 一次。每次先测量无挡光板时光谱仪在参考板正上方(光谱仪距离参考板的高度应使参考板充满光谱仪视 场，且参考板上无仪器阴影存在)测到的总辐射量 L_{G1}，接着用挡光板挡住太阳直射光测得漫射辐射量 L_d，再移开挡光板测量总辐射量 L_{G2}，L_d 与 L_{G1} 和 L_{G2} 的平均值之比即是测量时刻的漫射辐射与总辐射比。

3　数据结果处理与分析

3.1　地表光谱数据处理与分析

对于 42 个地面采样点，将每个采样点的 10 次测量和前后 4 次白板测量数据分别进行平均，得到该采样点的地面和白板的平均计数值，将参考板 BRF 按测量时刻太阳天顶角进行插值计算得到参考板的双向反射比，根据式(10)，计算获得每个采样点的地表绝对反射比$\rho(\lambda)$。

$$\rho(\lambda)=\frac{v_T(\lambda)}{v_s(\lambda)}\rho_s(\lambda) \tag{10}$$

式中，$\rho_s(\lambda)$为参考板 BRF 插值得到的测量时刻的参考板双向反射比，$v_s(\lambda)$和 $v_T(\lambda)$分别为参考板和测量目标的平均计数值。

将 42 个采样点的绝对反射比进行平均得到场地的地表绝对反射比，场地的地表绝对反射比结果如图 3。可以看出，二连浩特场地在可见光-近红外的光谱反射比数据在 0.1—0.4 之间，反射比随波长的增加平稳递增。地表反射比在 350—1100nm 范围的平均相对差异分别为 3.1%，表明实验场地表反射离散度小，场地光学均一性好。对 42 个采样点数据获取的卫星过境前后 1h 内的测量数据得到的地面绝对反射比与卫星过境时刻对应地面点的绝对反射比进行比较，其相对差异只有 0.3%，说明利用卫星过境前后 1h 测量得到的反射比作为场区的反射比具有代表性。利用地面反射率光谱数据与 MODIS 波段光谱响应函数卷积，获得 MODIS 对应波段的地面等效反射率，等效反射率的计算误差 0.004—0.02，平均精度为 3.3%。

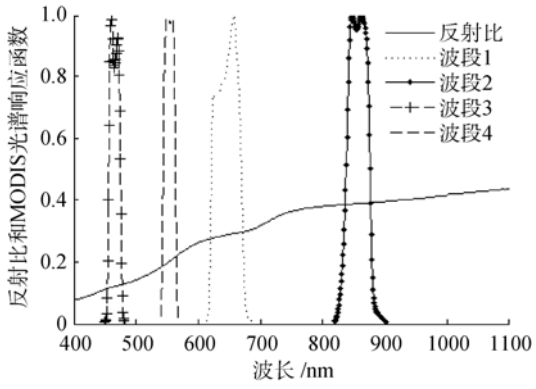

图 3　二连浩特沙地反射比和 MODIS 光谱响应函数

© 1994-2012 China Academic Journal Electronic Publishing House. All rights reserved.　http://www.cnki.net

3.2 大气光学特性数据处理

根据 CE318 测量的直射太阳辐射和天空辐射数据，采用 Langley 方法计算所有波段大气总光学厚度和气溶胶光学厚度，计算误差为 0.5%。图 4(a)显示 2007-06-01 CE318 数据各波段拟合的 Langley 曲线，可以看出：测量结果的线性较好，自 7:30—19:00 点测量期间气溶胶含量变化很小，大气状况很稳定。图 4(b)显示 Junge 参数 α 和 β，可以看出，观测当天实验场区以大粒子气溶胶为主，气溶胶浓度很低，大气晴朗稳定，能见度很好，气溶胶对辐射传输的影响很小。根据卫星过境时间，对计算的上午时段的系列大气总光学厚度进行内插得到卫星过境时刻大气总光学厚度，再与 MODIS 波段光谱响应函数卷积得到 MODIS 波段大气总光学厚度。

3.3 漫射辐射与总辐射比计算与分析

辐照度法定标的重要参数是卫星过境时刻太阳天顶角方向 θ_s 和卫星天顶角 θ_v 方向的漫射辐射与总辐射之比。如果卫星过境时刻没有进行漫射辐射与总辐射测量，或者卫星观测天顶角很小，未在太阳天顶角变化范围之内，需要将一系列测值按照下式内插或外推 θ_s 和 θ_v 时的 α_s 和 α_v (Biggar, 1990)，

$$\log\left(\frac{E_D}{E_G}\right)=\log(1-\alpha)=\log(1-\rho s)-(1-b)\delta/\mu_s \quad (11)$$

式中，大气质量 $m=1/\mu_s$，上式可简化为线性公式 $y=y_0+cm$，斜率 c 为 $-(1-b)\delta$，截距 y_0 为 $\log(1-\rho s)$。先确定当天大气是否稳定，从测量数据绘出的对数图 5 可以看出，$\log(1-\alpha)$随大气质量减小而增加，亦即漫射辐射与总辐射之比随大气质量减少而减少，证明当天大气稳定，与 CE318 测量结果吻合。这样经数据拟合出斜率，从而算出 θ_s 和 θ_v 时的 α_s 和 α_v。

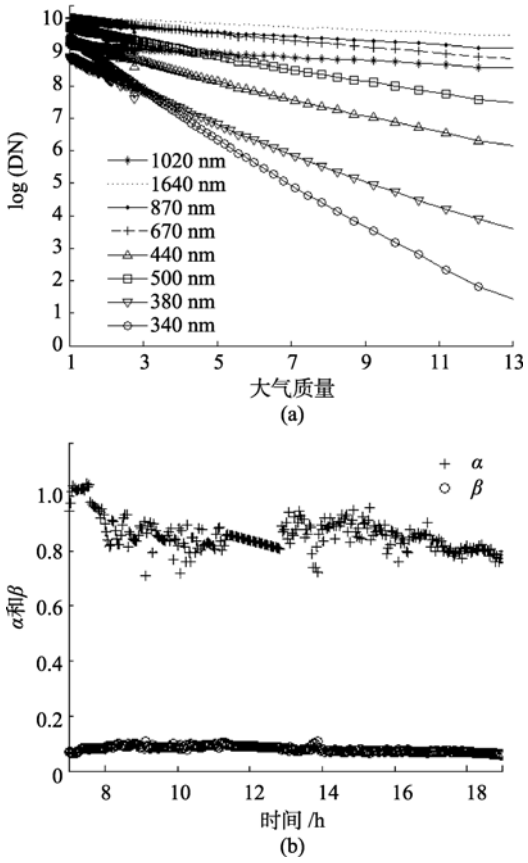

图 4 2007-06-01 大气光学特征
(a) CE318 各波段数据的 Langley 曲线; (b) 波长指数 α 和浑浊系数 β

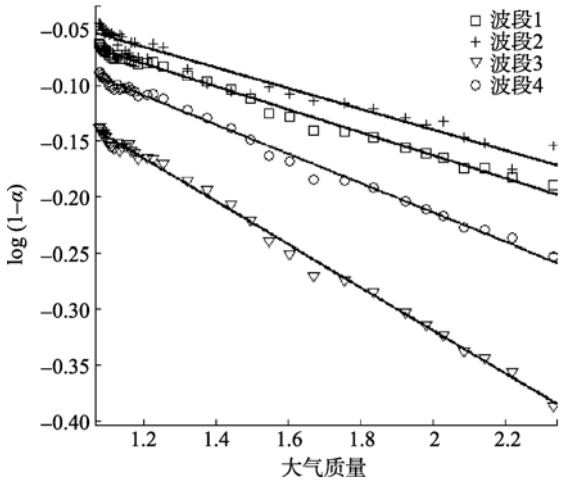

图 5 对数图(log(1−α)对 m)

3.4 定标系数计算与分析

将 MODIS 波段对应的地面反射率、气溶胶光学厚度、水汽含量、臭氧含量以及太阳和卫星几何参数等输入到 6S 辐射传输模型，计算获得大气内反射率 ρ_A 和球面反照率 s。将这 2 个参数与地面反射率、大气总光学厚度以及卫星过境时太阳天顶角方向和卫星天顶角方向的漫射辐射与总辐射之比带入式(8)，即可计算出卫星过境时 MODIS 各波段的表观反射率。利用 GPS 数据进行星—地同步观测实验场区精确配准，提取 MODIS 传感器图像对应地表实验场区的像元平均计数值。由于 MODIS 波段空间计数值为零(即偏移量 offset=0)，则利用式(12)获得各波段定标系数。

$$\rho_i = C_i \times \mathrm{DC}_i \quad (12)$$

式中，ρ_i 为 MODIS 波段 i 的表观反射率；DC_i 是 MODIS 波段 i 图像对应地表实验场区的像元平均计数值；C_i 是 MODIS 波段 i 的定标系数。

以 MODIS 的星上定标为标准，检验辐照度法定标的结果，同时与当天利用反射率基法定标得到

© 1994-2012 China Academic Journal Electronic Publishing House. All rights reserved. http://www.cnki.net

的结果进行比较。表 1 是辐照度法定标、反射率基法定标及星上定标获得的 MODIS 各波段定标系数。

表 1　2007-06-01 辐照度法、反射率法及星上定标比较

	波段 1	波段 2	波段 3	波段 4
辐照度法: ρ_{TOA}	0.249	0.344	0.150	0.185
反射率法: ρ_{TOA}	0.253	0.351	0.154	0.189
星上定标: ρ_{TOA}	0.250	0.355	0.152	0.189
辐照度法: $C_l/\times10^{-5}$	5.25	3.17	3.78	3.4
反射率法: $C_l/\times10^{-5}$	5.33	3.24	3.87	3.46
星上定标: $C_l/\times10^{-5}$	5.27	3.27	3.82	3.47
辐照度法与星上定标相对差异(%)	−0.392	−3.244	−0.872	−2.080
反射率法与星上定标相对差异(%)	0.999	−1.009	1.304	−0.247

从表 1 定标结果看出，辐照度法得到的表观反射率与 MODIS 星上定标和反射率基法定标结果具有很好的一致性，定标结果与星上定标结果相对差异小于 3.3%，肯定了辐照度法的正确性。在 3 种方法辐照度法得到的表观反射率值最低，且辐照度法与星上定标的相对差异中第 2、4 波段的误差要比第 1、3 波段大，原因在于地面漫射辐射与总辐射测量过程中，由于挡光板的操作误差导致测量的漫射辐射量偏小，使计算出的漫射辐射与总辐射之比偏小，从而使结果偏低，第 2、4 波段漫射辐射与总辐射的比值相对于其他波段更小些，导致这 2 个波段值差异偏大。以上证明：在辐照度法中，漫射辐射与总辐射比的测量对辐照度法的精度影响很关键，通过更精准的仪器测量漫射辐射与总辐射之比可以提高辐照度法的精度。

为了研究气溶胶的假设对辐照度法和反射率基法两者结果影响的不同，利用 2007-06-01 在二连浩特实验场的地面实测数据，选择沙漠型、大陆型、城市型 3 种不同的气溶胶模式计算表观反射率，结果如图 6。由此得到的定标系数如表 2。结合图 6 和表 2 可以看出，在沙漠型、大陆型、城市型等 3 种不同的气溶胶模式下，辐照度法和反射率法得到的定标系数受到了不同的影响。在 3 种气溶胶模式下，辐照度法得到的表观反射率变化很小，表观反射率差异仅为 0.25%，误差范围为 0.39%—3.78%。由于气溶胶模式的假设只对 ρ_{A} 和 s 产生影响，而这 2 个值很小，辐照度法采用漫射辐射与总辐射之比实测值代替对气溶胶模式的假设，致使气溶胶模式的假设对辐照度法影响很小；而不同的气溶胶模式对反射率基法的结果影响很大，表观反射率差异达 1.7%，误差范围 0.47%—8.96%，城市型气溶胶模式由于具有强吸收，致使表观反射率最小。这说明辐照度法可以减小因气溶胶模式的假设产生的误差。

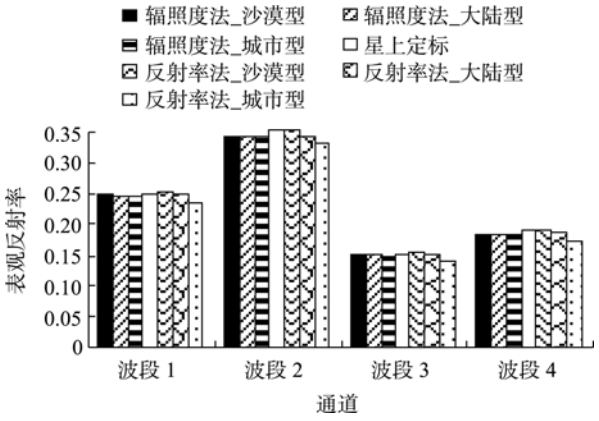

图 6　不同气溶胶模式下反射率法和辐照度法结果对比

表 2　不同气溶胶模式得到的定标系数比较

定标系数	辐照度法_沙漠型 $/\times10^{-5}$	5.25	3.17	3.78	3.40
	辐照度法_大陆型 $/\times10^{-5}$	5.22	3.15	3.78	3.38
	辐照度法_城市型 $/\times10^{-5}$	5.19	3.15	3.71	3.35
	星上定标/$\times10^{-5}$	5.27	3.27	3.82	3.47
	反射率法_沙漠型 $/\times10^{-5}$	5.33	3.24	3.87	3.46
	反射率法_大陆型 $/\times10^{-5}$	5.24	3.18	3.83	3.40
	反射率法_城市型 $/\times10^{-5}$	4.92	3.04	3.54	3.16
辐照度法与星上定标误差范围/%		0.39—1.51	3.19—3.78	0.87—2.69	2.05—3.35
反射率法与星上定标误差范围/%		0.6—6.71	2.88—6.98	0.47—7.34	1.93—8.96

4　结　论

2007-06-01 在二连浩特开展的 Terra 卫星 MODIS 可见光–近红外波段的辐照度定标研究，得到以下结论：

(1) 通过本次辐照度法定标，获得 MODIS 各波段的辐射定标系数，与星上定标及场地反射率法定标比较表明，辐照度法和 MODIS 的星上定标和反射率法定标结果一致性很好，相对差异小于 3.3%，肯定了辐照度法的正确性；

(2) 辐照度法中，漫射辐射与总辐射比的测量对辐照度法的精度影响很关键；

(3) 辐照度法采用漫射辐射与总辐射的实测比值代替对气溶胶模式的假设，气溶胶模式的假设只对 ρ_{A} 和 s 产生影响，减小了因气溶胶模式的假设产生的误差；

© 1994-2012 China Academic Journal Electronic Publishing House. All rights reserved.　http://www.cnki.net

(4) 本文为光学遥感采用辐照度法进行定标提供了一个较为系统的试验技术流程与方法途径。

致 谢 此次实验数据的获取得到中国科学院遥感应用研究所魏飞鸣、傅鹤、朱利、胡梅、郭丁、肖丹涛等同志的帮助，国家气象局气象卫星中心胡秀清在数据计算方法上给予了帮助，在此表示感谢！

REFERENCES

Biggar S F. 1990. Cross Methods for Satellite Sensor Absolute Radiometric Calibration. America: the University of Arizona

Biggar S F, Dinguirard M C, Gellman D I, Henry P, Jackson R D, Moran M S and Slater P N. 1991. Radiometric calibration of SPOT 2 HRV: a comparison of three methods. Proc.SPIE, **1493**: 155—162

David C H. Analytical spectral devices.2002. Inc. HandHeld Spectroradiometer User's Guide

Dinguirard M and Slater P N. 1999. Calibration of space-multispectral imaging sensors: a review. *Remote Sensing of Environment*, **68**: 194—205

Gu M L. 2000. In-flight absolute radiometric calibration of satellite remote sensor. Spacecraft Recovery & Remote Sensing, **21**(1): 16—21

Hu X Q, Zhang Y X and Qiu K M. 2003. In-flight radiometric calibration for VIR channels of FY-1C satellite sensor by using irradiance-based method. *Journal of Remote Sensing*, **7**(6): 458—464

Li X Y. 2006. In Flight Radiometric Calibration and Pixel Based Calibration for CCD Camera and WFI Imager on CBERS-02. Beijing: Chinese Academy of Sciences

Qiu K M. 2001. Constructions, Scientific fruits and applied foreground of Chinese satellite radiometric calibration sites. Corpus Chinese Remote Sensing Satellites Radiometric Calibration Sites Contribution. Beijing: Ocean Press

Richard D M. What is the total column ozone amount over your house?http://toms.gsfc.nasa.gov/teacher/ozone_overhead_v8.html. [2008-09-09]

Slater P N, Biggar S F, Holm R G, Jackson R D, Mao Y, Moran M S, Palmer J M and Yuan B. 1987. Reflectance- and radiance-based methods for the cross absolute calibration of multispectral sensors. *Remote Sensing of Environment*, **22**(1): 11—37

Thome K J. 1999a. Validation plan for MODIS level 1 at-sensor radiance. http://modis.gsfc.nasa.gov/data/atbd/val_atbd.php [2008-09-09]

Thome K J, Crowther B G and Biggar S F. 1997b. Reflectance- and irradiance-based calibration of Landsat-5 Thematic Mapper. *Canadian Journal of Remote Sensing*, **23**: 309—317

Tian Q J. 1999. Quantitative theory, Method and application of remote sensing information. China Science & Technology Publishing House

Xiong X and Barnes W. 2006. An overview of MODIS radiometric calibration and characterization. *Advances in Atmospheric Sciences*, **23**(1): 69—79

Yuan H J, Gu X F, Chen L F, Yu T, Liu Q and Li X W. 2006. Retrieval and analysis of aerosol optical thickness over Qianyanzhou Region. *Journal of Remote Sensing*, **10**(5): 762—769

Zhang D Y, Qiao Y L, Yi W N. Yang S Z, Meng F G, Wu H Y and Zhang J P. 2002. The irradiance-based method research of experimentation on radiometric calibration site-the comparison of synchronous observing instruments. *Optoelectronic Technology & Information*, **15**(3): 9—13

附中文参考文献

顾名澧. 2000. 星载传感器在飞行时的绝对辐射定标方法. 航天返回与遥感, **21**(1): 16—21

胡秀清, 张玉香, 邱康睦. 2003. 采用辐照度法对 FY-1C 气象卫星可见近红外波段进行绝对辐射定标. 遥感学报, **7**(6): 458—464

李小英. 2006. CBERS-02 卫星 CCD 相机与 WFI 成像仪在轨辐射定标与像元级辐射定标研究. 北京: 中国科学院

邱康睦. 2001. 中国遥感卫星辐射校正场建设和科研成果及其应用前景. 中国卫星遥感辐射较正场科研论文选编

田庆久. 1999. 遥感信息定量化理论、方法与应用. 遥感知识创新文集

袁海军, 顾行发, 陈良富, 余涛, 刘强, 李小文. 2006. 江西千烟洲地区气溶胶光学厚度的反演与分析. 遥感学报, **10**(5): 762—769

张冬英, 乔延利, 易维宁, 杨世植, 孟凡刚, 吴浩宇, 章俊平. 2002. 基于辐照度法的场地辐射校正试验研究——场地同步观测仪器的比较. 光电子技术与信息, **15**(3): 9—13

© 1994-2012 China Academic Journal Electronic Publishing House. All rights reserved. http://www.cnki.net